NEUTRAL ATOM MODELING OF THE TFTR FIRST WALL, PUMP DUCTS, AND NEUTRAL BEAMS

PLASMA ENGINEERING

KEYWORDS: *neutral atom, TFTR, first wall*

LISA A. HAYNES, J. P. KELLY, and DAVID N. RUZIC*
University of Illinois, 100 Nuclear Engineering Laboratory
103 South Goodwin Avenue, Urbana, Illinois 61801

DENNIS MUELLER and J. KAMPERSCHROER
Princeton Plasma Physics Laboratory, Princeton, New Jersey 08543

Received August 5, 1996
Accepted for Publication March 11, 1997

The DEGAS neutral transport code is used in two separate cases to simulate the neutral beam box and vessel of the Tokamak Fusion Test Reactor (TFTR). For the neutral beam box simulation, known input parameters include the ion density at the source exit and the proportion of input gas that is converted to the high-energy atomic beam. The T^0 current to the torus is $(1.61^a \pm 0.03) \times 10^{20}$ s^{-1}, with the high-energy beam having a median energy above 95 keV. Corresponding results are found for the D^0 current. In addition, the amount of gas reaching the torus, the pressure, and the flux and energy distributions of the ions and neutrals to the walls are found. For the tritium case, it is calculated that 92.4 ± 0.2% of the input tritium reaches the cryopanels, 6.64 ± 0.05% reaches the torus, and 1.0 ± 0.2% reaches the ion dump. In the second run, DEGAS was used to calculate the neutral atom flux and energy of particles incident on the walls of the vacuum vessel and the neutral pressure in the pump duct of TFTR during a typical supershot with a 50/50 mixture of deuterium-tritium. Output quantities are the current and energy to the bumper limiter and first wall. The total amount of tritium implanted in the vacuum vessel after 150 shots of 1-s duration is estimated to be 0.5 ± 0.1 g in the bumper limiter and 0.042 ± 0.023 g in the outer wall and pumping duct, which is well within the 5-g on-site inventory and the 2-g in-vessel inventory. The implications of these results are discussed.

I. INTRODUCTION

Deuterium-tritium experiments commenced in the Tokamak Fusion Test Reactor (TFTR) on December 10, 1993, with 6 MW of fusion power being produced.[1] Subsequent experiments extended this value to >10 MW (Ref. 2). An essential component in these high fusion power experiments was the use of tritium ($t_{1/2}$ = 12.3 yr), the radioactive isotope of hydrogen. Currently, TFTR is the world's only magnetic confinement experiment utilizing this hydrogenic isotope. Inherent in the use of tritium are certain regulatory constraints: The maximum quantity allowed on the TFTR site at any time is small, 5 g, of which up to 2 g may be in a releasable form in the tokamak vacuum vessel. Because of the importance of ascertaining the quantity of tritium retained in the system, experimental time on TFTR has been devoted to tritium retention and recycling experiments.[3,4] Modeling key components of the system can yield important information pertinent to tritium retention, as well as providing insight for future devices. To this end, separate computer simulations of the tritium inventory in the neutral beamline and in the torus vacuum vessel have been performed using the DEGAS computer code.

*E-mail: druzic@uiuc.edu

II. TFTR NEUTRAL BEAM OPERATIONAL EXPERIENCE

The TFTR neutral beam injection system has been described in detail elsewhere[5,6] and will only be summarized here. Each of the four neutral beamlines possess three ion sources,[7] any of which may be operated in deuterium or tritium independent of the others. In the sources,

ions are accelerated from a plasma through a series of four grids up to a maximum energy of 120 keV. Typical deuterium operation is in the range of 90 to 100 keV, whereas tritium operation is generally higher, 100 to 110 keV. For this study, the energy is taken to be the maximum value of 120 keV, which does not significantly alter the results because of the similarity of the cross sections at those energies.

In the low power discharge that creates the plasma from which the ion beam is extracted, three hydrogenic ions are produced: For deuterium (or tritium), these are D^+ (T^+), D_2^+ (T_2^+), and D_3^+ (T_3^+). After acceleration, the ion beam enters a gas neutralizer where collisions convert a portion of the ion beam to neutrals. During this process, practically all of the molecular ions dissociate. Without loss of applicability to the tritium inventory question, the incident D_2^+ (T_2^+) and D_3^+ (T_3^+) molecular ions are treated as 2 D^+ (T^+) and 3 D^+ (T^+) at one-half and one-third of the acceleration energy, respectively.

With this simplification, the charge-exchange simulation need only consider D^+ (T^+) and D^0 (T^0). The system of coupled differential equations[8] then reduces to

$$\frac{df_{D^+}}{d\pi} = \sigma_{01} f_{D^0} - \sigma_{10} f_{D^+} \quad (1)$$

and

$$\frac{df_{D^0}}{d\pi} = \sigma_{10} f_{D^+} - \sigma_{01} f_{D^0}, \quad (2)$$

where f_{D^+} and f_{D^0} are the D^+ and D^0 fractions of the beam, respectively; σ_{01} and σ_{10} are the electron stripping and electron capture cross sections for D^0 and D^+; and π is the integral density n of the gas through which the beam is passed. These two equations have the following solutions:

$$f_{D^+} = \frac{\sigma_{01}}{\sigma_{01} + \sigma_{10}} + \frac{\sigma_{10}}{\sigma_{01} + \sigma_{10}} \exp[-(\sigma_{01} + \sigma_{10})\pi] \quad (3)$$

and

$$f_{D^0} = \frac{\sigma_{10}}{\sigma_{01} + \sigma_{10}} \{1 - \exp[-(\sigma_{01} + \sigma_{10})\pi]\} , \quad (4)$$

where

$$\pi = \int_{beampath} n.dl .$$

After neutralization, any remaining charged particles are removed from the beam by a deflection magnet. The discarded ions are deposited onto separate water-cooled ion dumps for the full-, half-, and third-energy D^+ (T^+). The resultant neutral beam is then available for transport to the tokamak.

Lining the two sides of the beamline are cryopanels, the innermost surfaces of which are maintained at liquid helium temperature, 4.5 K. Here, 30 m^2 of cryopanels differentially pump the beamline with a total pumping speed of $\sim 10^6$ ℓ/s for deuterium. This large pumping speed is necessary to maintain the pressure at or below 10^{-5} Torr, in the presence of a total gas input of 100 Torr·ℓ/s, to prevent excessive charge-exchange (and subsequent loss) of the neutral beam along its path from the magnet to the torus.

A summary of the gas and power efficiencies of the deuterium and tritium neutral beams are given in Table I. The extracted current at a given voltage is less for tritium than it is for deuterium. This is due to the fact that the ion sources will only operate over a narrow range of perveance (where perveance is a quantity, for a given accelerator configuration, that is proportional to the extracted ion current and inversely proportional to the acceleration potential[9] times the square root of the mass of the extracted ions). At 120 keV, ~70 A of ions can be extracted from a deuterium plasma compared with 60 A from tritium.

Beam composition (species) of the extracted ion beams has been measured spectroscopically[10] and typical values used in the table. Gas requirement is the flux of thermal D_2 or T_2 necessary to create the extracted currents, $F_{0\infty}$ and $F_{+\infty}$ are the equilibrium neutral and ion fractions of the beam. It is assumed that the ion and neutral fractions are no longer changing with π; i.e., π is taken to be infinite in Eqs. (3) and (4). It has been found that a significant fraction of the extracted particles are widely divergent and lost close to the ion source.[11] This loss is reflected by the transmission efficiency column in Table I. This loss is taken into account in the neutral and ion currents and in the power calculation.

Gas is supplied to a location in the neutralizer that has equal conductance to cryopanels and to the plasma source. No separate gas feed into the plasma source is provided. In deuterium, the average gas flow rate for the 12 ion sources is 41 ± 3 Torr·ℓ/s and in tritium 33 ± 2 Torr·ℓ/s. The quantity of gas contained in the extracted 70 A and 60 A of D^+ or T^+ is 8.4 and 7.1 Torr·ℓ/s, respectively. The instantaneous gas efficiency for such operation is 20%. Gas is pulsed prior to beam extraction, and the gas efficiency over the entire beam cycle is <20%. Taking into account the gas lead in time of 0.5 s prior to establishment of the arc and 0.5 s of arc prior to beam extraction, the tritium gas efficiency for a 1-s beam pulse is 10%. This average value is a function of pulse length. As shown by the DEGAS modeling described in Sec. III, only a fraction of the extracted ions, however, are injected into the torus as neutrals. The gas throughput corresponding to the 4.07 MW of injected T^0 is 4.2 Torr·ℓ/s. Instantaneous and pulse-averaged gas efficiencies are 13 and 6%, respectively. Of the tritium injected into the neutral beamlines, 6% makes it as fuel to the torus; the remaining 94% is pumped on the cryopanels. Of the tritium

TABLE I

Experimental Gas Requirements and Currents and Analytical Efficiency, Fractions, and Powers of Deuterium and Tritium in the TFTR Beam Boxes*

Species	Species Fraction	Extracted Current (A)	Gas Requirement (s)	$F_{0\infty}$	Neutral Current (A)	Transmission Efficiency	Injected Power (kW)	$F_{+\infty}$	Ion Current (A)	Power to Ion Dumps (kW)
D^+	0.72	50.4	1.58×10^{20} D_2	0.44	22.2 D_0	0.83	2209	0.56	28.2 D^+	2811
D_2^+	0.21	14.7	9.19×10^{19} D_2	0.725	21.3 D_0	0.83	1061	0.275	4.0 D^+	403
D_3^+	0.07	4.9	4.59×10^{19} D_2	0.82	12.1 D_0	0.83	400	0.18	0.9 D^+	88
Total			2.95×10^{20} D_2 (8.4 Torr·ℓ)				3670			3302
T^+	0.72	43.2	1.36×10^{20} T_2	0.625	27.0 T_0	0.83	2689	0.375	16.2 T^+	1614
T_2^+	0.23	13.8	8.63×10^{19} T_2	0.82	22.6 T_0	0.83	1127	0.18	2.5 T^+	247
T_3^+	0.05	3.0	2.81×10^{19} T_2	0.85	7.7 T_0	0.83	254	0.15	0.5 T^+	45
Total			2.49×10^{20} T_2 (7.1 Torr·ℓ)				4070			1906

*For deuterium, there are 70 A of ions extracted at 120 kV (8400 kW). The gas feed rate is 41 Torr·ℓ/s. For tritium, there are 60 A of ions extracted at 120 kV (7200 kW), with a gas feed rate of 33 Torr·ℓ/s.

injected into the beamline, 2% reaches the ion dump in the form of energetic tritons, and another ~2% is lost near the ion source as highly divergent particles. We assume that these beam-absorbing surfaces are saturated with hydrogenic gas, and the associated 4% of the gas flux striking the interior beamline surfaces is included in the 94% reaching the cryopanels.

Of 7.2 MW of extracted tritium ion power at 120 keV, 4 MW (or 55%) is injected into the torus, 1.9 MW (26%) reaches the ion dumps, and 1.2 MW is lost as highly divergent particles. For deuterium only 44% of the extracted power usefully heats the plasma. This is the result of the higher particle velocities and concomitantly lower charge-exchange efficiency. Of the extracted deuterium power, 39% is dissipated on the ion dumps. Tritium injection is much more efficient than deuterium as is seen by the fact that even though less current is extracted, more neutral power is injected. A more pronounced beneficial effect is in the power delivered to the ion dump. The residual ion power for tritium is <60% that for deuterium. Since the full-energy ion dump is currently the limiting constraint due to power handling in the pulse lengths allowed for injection, longer pulses are permissible in tritium.

III. DEGAS SIMULATION

DEGAS (Refs. 12 and 13) is a three-dimensional Monte Carlo neutral species code containing extensive atomic physics. The simulation includes charge-exchange, electron and ion impact ionization, molecular dissociation, and recombination. Energy and angle-resolved wall reflection coefficients are taken from the VFTRIM code,[14,15] which takes into account the effects of surface roughness. The grid coordinates of the simulation are input to the code, and values for electron and ion temperature, density, velocity, and species are included for each grid cell. Particles are moved using a pseudocollision algorithm. Several input parameters exist, such as types of reflection, volume sources (as in gas puffing) or currents (as in reflection off the bumper limiter), and run length parameters. During the simulation, the DEGAS code follows neutral particles until they are lost to an exit, are ionized, or have too low a weighting. Included in the output are neutral gas densities, pressure, fluxes, ionization rates, momentum transfer rates, energy transfer rates, power loads to the wall, and wall erosion rates.

III.A. Neutral Beam Simulation

Knowing the macroscopic quantities found experimentally and analytically in Sec. II, the process was modeled with DEGAS to determine the detailed neutral behavior and gain knowledge of the plasma in the source. Tritium is followed from injection into one of the four neutral beamlines until it is lost on a cryopanel, ion dump, or injected into TFTR. The beamline is modeled as possessing only one ion source and neutralizer rather than three independent units. Relevant quantities are trebled to account for this simplification. A two-dimensional simulation of the geometry is used. To simulate the three-dimensional geometry of the beamline, the ion dump is transposed from the top of the beamline to the side. To

account for the lost cryopanel area, an equivalent area of the front of the box is taken to be cryopanel. The resultant DEGAS geometry, with a 61 × 40 mesh, is shown in Fig. 1. Each of the three beam species were simulated with separate DEGAS runs.

The D^+ and T^+ ion densities n at the ion source exit were estimated in the following way:

$$n = \frac{I}{Av} ,$$

where I is the current in ions per second, A is the area of the beam, and v is the velocity. This calculation yields a D^+ (120-keV) estimate of 1.78×10^9 ion/cm^3. Source densities and temperatures were estimated by iterating the values so as to attain the correct ion fluxes to the ion dump and torus. The electron and ion densities in the source were found in this manner to be 1×10^{13}/cm^3. These densities however, are only known to within a factor of 2 because of the weak dependence of the result on the electron and ion densities in the source. The electron density in the neutralizer was 5×10^{11}/cm^3. Electron and ion temperatures in the source were found to be 10 and 1 eV, respectively.

The D_2 and T_2 flow rates to each source used in this simulation are 30 Torr·ℓ/s and 27 Torr·ℓ/s, respectively.[9] These values correspond to total deuterium and tritium atomic currents of 6.36×10^{21} and 5.72×10^{21} s^{-1}, respectively. The values described in Sec. II typically range 25% higher. One estimate puts the power input to each simulated source at 7.8 MW (Ref. 16). For the case of the pure 120-keV D^+ beam, this translates to 1.2×10^{21} ion/s. This implies that ~19% of the neutral D_2 gas will eventually be ionized and extracted. It may be estimated that about half of the input gas will enter the source on the basis of geometry, implying that less than half of the gas that does reach the source will be ionized.

Once the ion density at the source exit was determined, the density of first-generation ions at a given point on the ion path, past the neutralizer region, was estimated to be

$$n_{D^+} = n_{D^+ neutexit} \exp\left(-\sigma \cdot \int dx_2 \cdot n_{D_2}\right) \quad (5)$$

and

$$n_{D^+} = n_{D^+ init}\left\{\frac{\sigma_{01}}{\sigma_{01}+\sigma_{10}} + \frac{\sigma_{10}}{\sigma_{01}+\sigma_{10}} \times \exp[-x_1 \cdot n_{D_2}(\sigma_{01}+\sigma_{10})]\right\} , \quad (6)$$

where

x_1 = path length inside the neutralizer (cm)

x_2 = path length through the rest of the beam box area (cm)

n_{D_2} = density of neutral gas (cm^{-3}) (assumed to be constant in each of the two separate regions)

σ = charge-exchange cross section (cm^2).

The charge-exchange cross section at 120 keV is 1.19×10^{-16} cm^2 in the deuterium-only case and 2.80×10^{-16} cm^2 in the tritium-only case.[8] By using Eqs. (5) and (6), the D^+ and T^+ first-generation ion densities were constructed over the entire ion path and input to DEGAS.

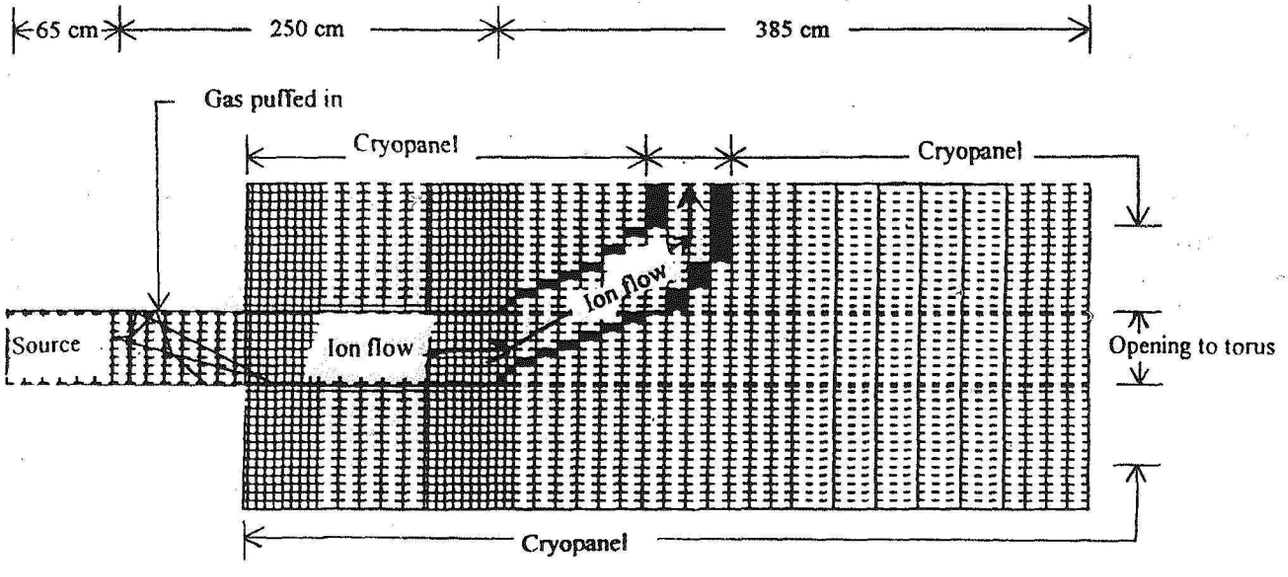

Fig. 1. DEGAS neutral beam box model and sample 20-particle DEGAS tritium flight.

Equation (5) determines the density between the neutralizer exit ($D^+_{neutexit}$) and the ion dump at the side of the beam box, and Eq. (6) determines the density between the source exit (D^+_{init}) and the neutralizer exit. There are also ions in areas outside the ion path recreated by stripping of a fast neutral. These are low magnitudes that introduce a second-order correction to the density—since the particle does not follow the ion path while it is a neutral—and have not been included here.

The DEGAS run for the neutral beam box simulation is then performed with all of the input as defined earlier for 20 and 5000 flight cases. A typical tritium flight track is shown in Fig. 1 from the 20-flight case. In this particular flight, the T_2 gas molecule is puffed in and undergoes several charge-exchange and recombination events before finally exiting our simulation region on its way to the torus as a high-energy neutral tritium atom (seen as the solid line near the top of the beamline). The details and data from a 5000-flight case (where flight tracks are not displayed) will be discussed in Sec. IV.

III.B. Torus Simulation

A simulation of TFTR deuterium-deuterium (D-D) supershot 55851 is performed. This particular shot was chosen because the current was high enough for good alpha confinement, it had a high central electron temperature, and many diagnostic results are available. This shot is characterized by a high D-D fusion yield and no magnetohydrodynamic (MHD) instabilities. The toroidal field was 5.1 T, the neutral beam injection (NBI) power was 24.6 MW, and the plasma current was ramped to 1.6 MA. The first wall was well conditioned, and a lithium pellet was injected prior to NBI (Ref. 17). The DEGAS model in this work differs from previous modeling of this supershot by Budny et al.[18] by including the pumping ducts and the conductances and modeling a 50/50 mix of deuterium and tritium. In addition, the proper mix of recycled D^0 and D_2 (and T^0 and T_2) from ion reflection from the inner bumper limiter is modeled. Neutral densities and fluxes to all surfaces can then be calculated. Pressures are compared with RGA and ion gauge readings for this supershot.

For this model, a grid was set up with 32 horizontal segments (that approximate the radial direction), which are parallel to surfaces of constant magnetic field lines, and 24 vertical segments (that approximate the poloidal direction) and are roughly orthogonal to the horizontal segments. The horizontal grid lines follow the magnetic field lines, except in and near the pumping duct, where the lines were altered to model the duct. Toroidal symmetry is assumed in this two-dimensional run. A conductance calculation was performed to model the remaining length of the duct to choose an exit size for the pump duct.

Figure 2 shows the grid used for the DEGAS simulation of TFTR. The grid is a vertical slice through the torus at the pumping duct. The center region is the core plasma and is not actually modeled in the DEGAS simulation. The core plasma is handled by the TRANSP code,[19] which calculates transport coefficients based on calculations using experimental data in the core plasma. In this case, supershot 55851 results were used.[20] The bumper limiter in the vessel extends from point A to point B and is considered to be carbon. The outer wall runs from point B to point C and the side of the pumping duct from point C to point D, both of which are stainless steel,

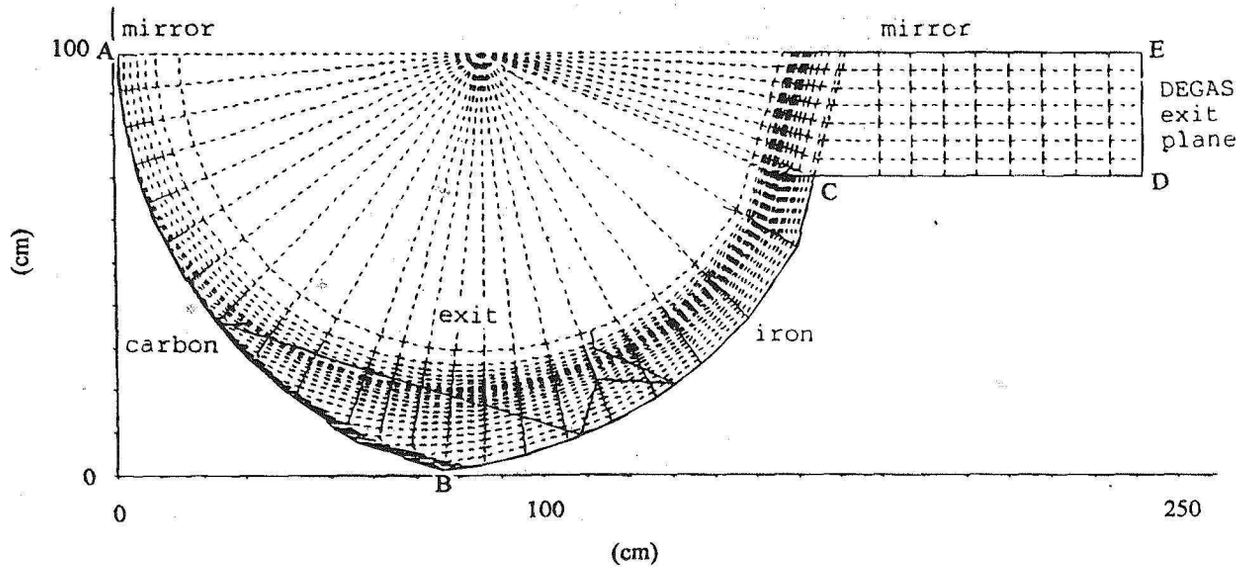

Fig. 2. DEGAS grid simulation.

and are modeled as iron. The end of the duct extends from point D to point E and contains an exit plane. The line from point E to point A is considered a mirror that reflects particles specularly. Additionally, a particle that reaches the center region is considered lost to the plasma.

The edge plasma parameters were obtained by iteration of DEGAS with the B2 code,[21] a two-dimensional fluid code, with the boundary between the core and the edge arbitrarily set at $r = 0.75$ m. Values for the electron density, electron temperature, ion temperature, diffusion coefficient, and electron and ion energy transport coefficients were extrapolated from TRANSP values at the boundary between the core and edge plasma. These results were modified to include the pumping duct and were used as input to the final simulation. The effects of including a volume source of deuterium and tritium at the entrance to the duct was also included to improve the statistics in this region.

IV. RESULTS

IV.A. Neutral Beam Run

The T_2 neutral density is shown in Fig. 3. The density is observed to be highest at the location just beyond the ion source. This is expected since it is here that the neutral gas is puffed in. The density then falls off quite rapidly through the neutralizer and finally reaches a near-equilibrium value for the rest of the beam box. The average T_2 density in the neutralizer (when summed over all three beam sources or T_1, T_2, T_3) is found to be $(6.0 \pm 0.5) \times 10^{13}$ cm^{-3} and $(1.1 \pm 0.2) \times 10^{12}$ cm^{-3} in the rest of the beam box. This corresponds to pressures of $(6.2 \pm 0.5) \times 10^{-4}$ Torr and $(1.1 \pm 0.2) \times 10^{-5}$ Torr, respectively. For the D_2 case, very similar results are found. Using these results in Eqs. (5) and (6), it is estimated that $15 \pm 2\%$ of the D^+ ions reach the ion dump,

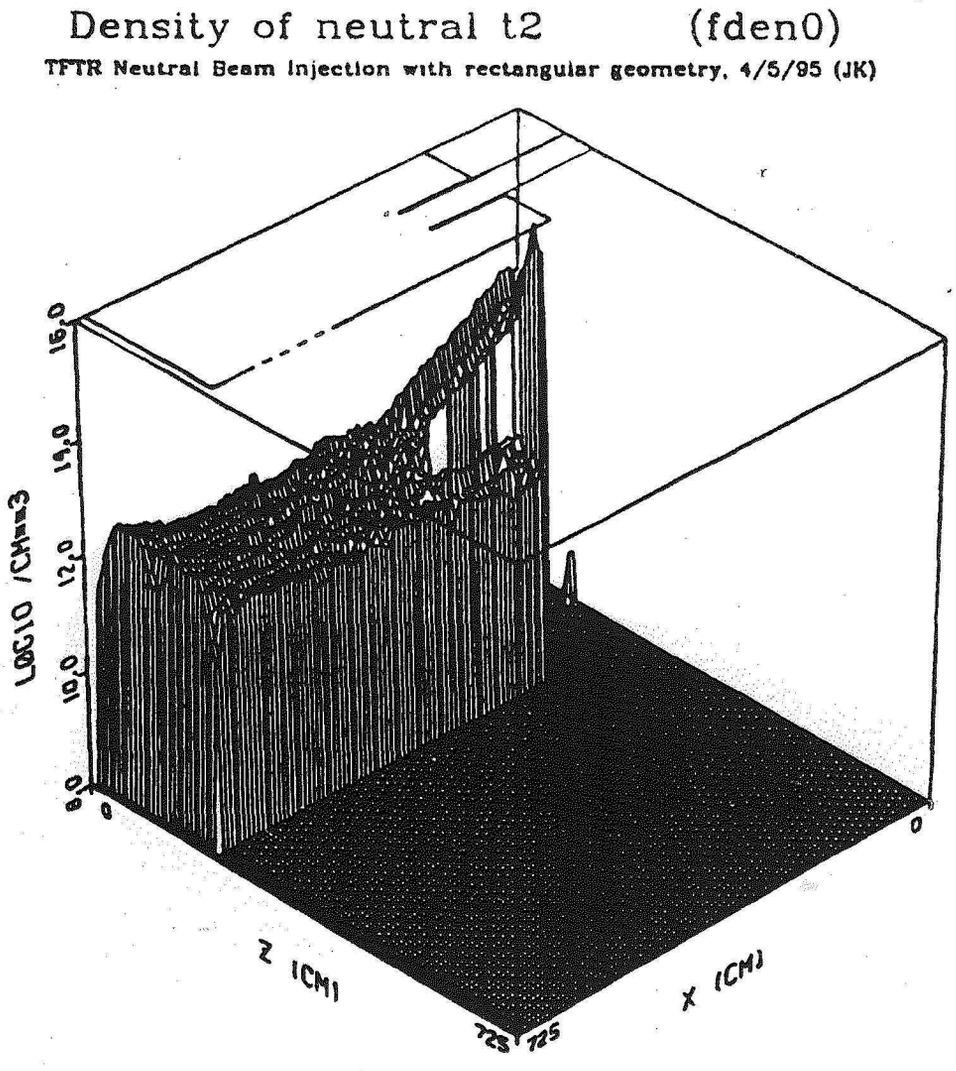

Fig. 3. Density of neutral T_2 in neutral beam box simulation.

while only 2 ± 1% of the T^+ ions reach the ion dump. This large disparity is the result of a much larger charge-exchange cross section for the tritium case. It has been observed in TFTR that neutralization of the tritium beams is more efficient than deuterium. This further explains why the heat loads to the ion dump are significantly lowered in the case of tritium operation.

The DEGAS energetic D^0 current to the torus is found to be $(1.72 \pm 0.03) \times 10^{20}$ s^{-1}, or 2.70 ± 0.05% of the input gas, with the average energy of the high-energy beam particles being 64 ± 1 keV. The corresponding energetic T^0 results are a current to the torus of $(1.61 \pm 0.03) \times 10^{20}$ s^{-1}, or 2.81 ± 0.05% of the input gas. The average energy for the high-energy beam particles was 76 ± 1 keV. The "average" energy is misleading, however, since it is being reduced by a relatively smaller number of low-energy particles. For both the deuterium and tritium beams, the median energy is found to be above 95 keV. The fractions of D_2 and T_2 (accelerated components of gas) in the beams were found to be 0.5 ± 0.2% and 0.6 ± 0.2% of particles in the beams, respectively. The discrepancy between these numbers and the total deuterium and tritium that is measured entering the torus and discussed in Sec. I, is the low-energy atomic and molecular flux that is estimated in the following discussion. The flux and energy distributions to the walls for the tritium run are shown in Table II. The errors on these values are as high as 50% as the values ranged greatly over individual zones.

Deuterium and tritium inventory is then taken. For the deuterium run, it was discussed previously that 2.70 ± 0.05% of the input gas reaches the torus. In addition, 6.23 ± 0.08% reaches the cryopanels and 0.36 ± 0.02% reaches the ion dump. The neutrals that DEGAS follows only accounts for 9.3 ± 0.1% of the gas pumped into sources. The remaining 90.7% of gas is now ionized and not followed by DEGAS. However, by using Eqs. (5) and (6), it is estimated that 3.3 ± 0.3% of the deuterium will be deposited on the ion dump as ions. This now leaves 87.4 ± 0.3% of the input current unaccounted. It is assumed that these ions will recombine by the end of the shot, and the places they are most likely to go are the torus and the cryopanels since the cryopanels at 4.5 K have a significantly higher sticking coefficient than the other internal wall surfaces. By simply taking area considerations, 95.8% of the unaccounted amount will reach the cryopanels, and the remaining 4.2% will reach the torus. The final distributions for both the deuterium and tritium runs are shown in Table III. These numbers compare reasonably well with estimates that ~95% of the input tritium current reaches the cryopanels, with the remaining 5% divided about equally between the torus and ion dump.

TABLE II

Neutral Flux and Average Energy to the Inside Surfaces of the Beam Box from DEGAS Calculations

	Total Neutral Flux to Wall ($cm^{-2} \cdot s^{-1}$)	Average Energy
Sides of box	2.03×10^{17}	0.65 keV
Front of box	1.64×10^{18}	42 keV
Rear of box	2.61×10^{16}	0.43 eV

TABLE III

Percentage of Injected Particles Reaching Various Areas as Calculated by DEGAS

	Deuterium	Tritium
Cryopanels	89.9 ± 0.3%	92.4 ± 0.2%
Torus	6.37 ± 0.05%	6.64 ± 0.05%
Beam dumps	3.7 ± 0.3%	1.0 ± 0.2%

IV.B. Torus Simulation

The deuterium and tritium ion fluxes to the bumper limiter are shown in Fig. 4, while the corresponding atomic fluxes are shown in Fig. 5. The distance on these graphs represents the distance from point A toward point B in Fig. 2. In both cases, the deuterium and tritium results were virtually identical, because of their similar masses, and the statistical errors are relatively small (on the order of a few percent). The peak in both the ion and atomic fluxes occurs ~0.3 m from point A. The neutral molecular fluxes to the bumper limiter were found to be relatively small, some three to four orders of magnitude smaller than the atomic and ion fluxes. The atomic deuterium and tritium fluxes to the outer wall are shown in

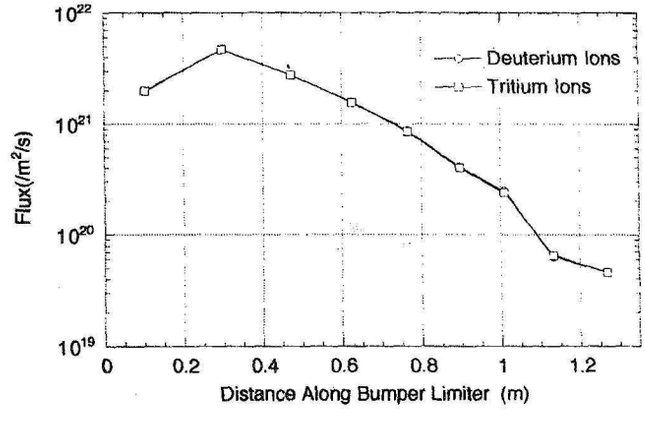

Fig. 4. Deuterium and tritium ion fluxes to the bumper limiter.

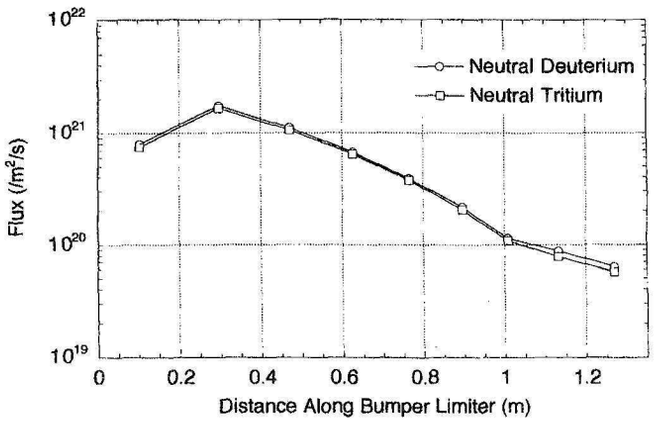

Fig. 5. Deuterium and tritium neutral fluxes to the bumper limiter.

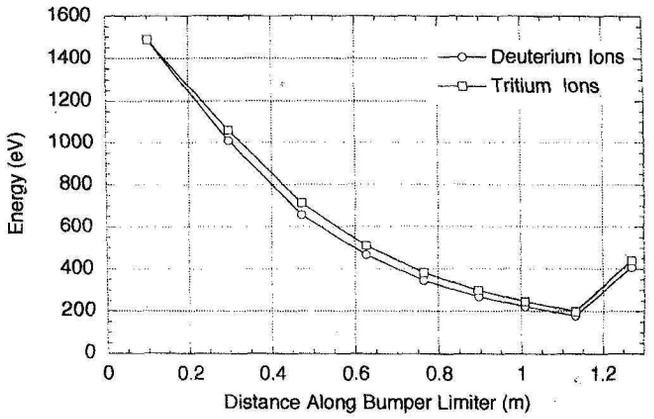

Fig. 7. Average energy of deuterium and tritium ions incident on the bumper limiter.

Fig. 6. The distance here represents the distance from point B toward point C in Fig. 2. Again, deuterium and tritium results are very similar, with the fluxes monotonically declining along the outer wall until we approach the pumping duct. Statistical errors are on the order of a few percent, except in a few extremely short wall segments.

Figure 7 shows the average energy of the deuterium and tritium ions incident upon the bumper limiter. The peak is seen to occur near point A and generally decrease as one approaches point B. The corresponding neutral results are shown in Fig. 8. The peak energy occurs near point B. Deuterium and tritium results are again similar in both cases. The energies of the molecules are very small (<0.2 eV). Figure 9 shows the average energy of atomic deuterium and tritium incident on the outer wall and pumping duct.

The pressure at the end of the pumping duct is found from DEGAS to be 1.35×10^{-5} Pa. This does not com-

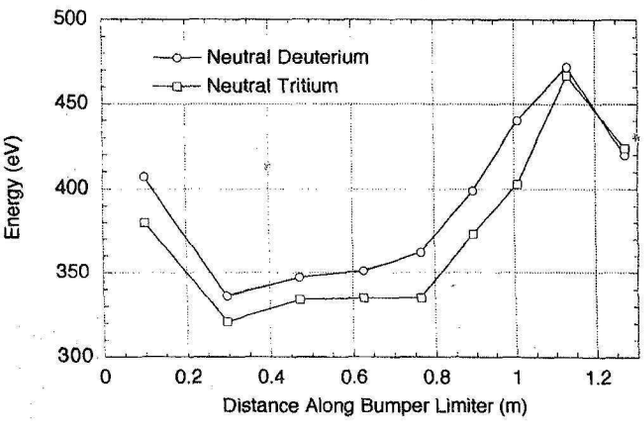

Fig. 8. Average energy of deuterium and tritium neutrals incident on the bumper limiter.

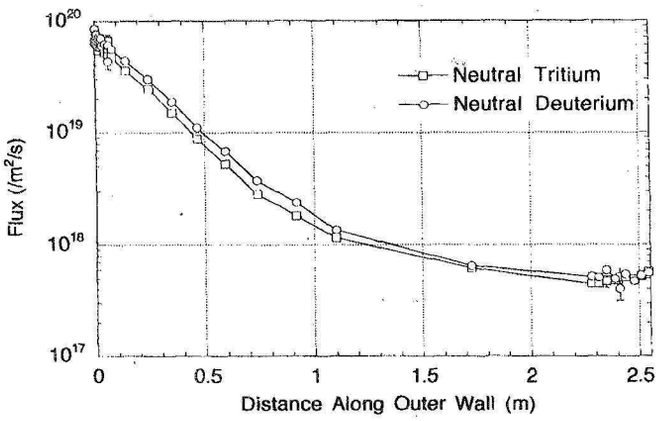

Fig. 6. Deuterium and tritium neutral fluxes to the outer wall and pumping duct.

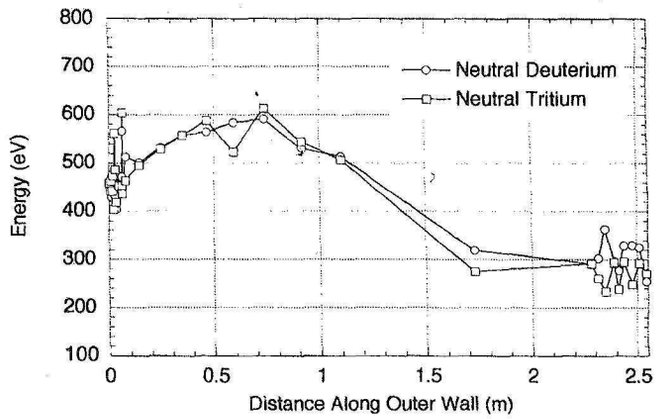

Fig. 9. Average energy of deuterium and tritium neutrals incident on the outer wall and pumping duct.

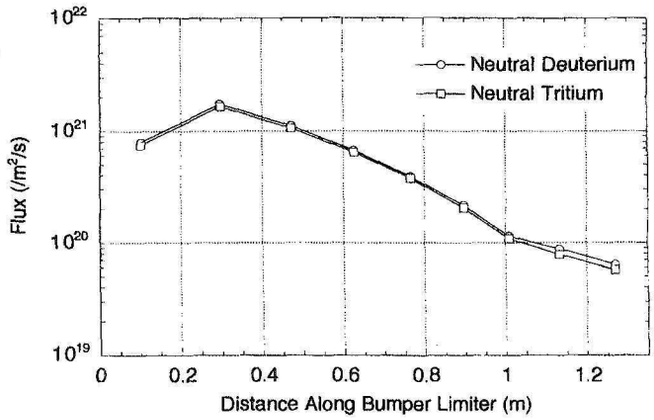

Fig. 5. Deuterium and tritium neutral fluxes to the bumper limiter.

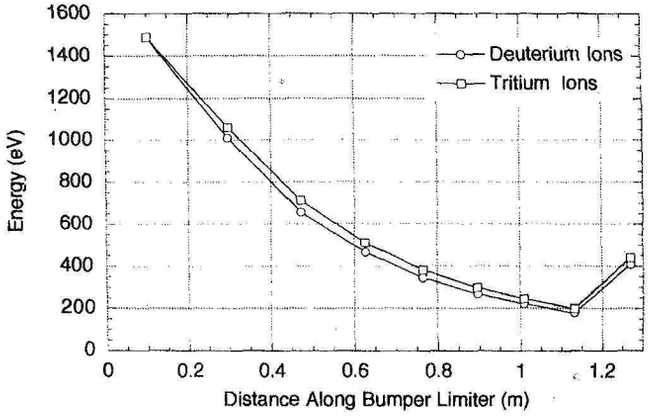

Fig. 7. Average energy of deuterium and tritium ions incident on the bumper limiter.

Fig. 6. The distance here represents the distance from point B toward point C in Fig. 2. Again, deuterium and tritium results are very similar, with the fluxes monotonically declining along the outer wall until we approach the pumping duct. Statistical errors are on the order of a few percent, except in a few extremely short wall segments.

Figure 7 shows the average energy of the deuterium and tritium ions incident upon the bumper limiter. The peak is seen to occur near point A and generally decrease as one approaches point B. The corresponding neutral results are shown in Fig. 8. The peak energy occurs near point B. Deuterium and tritium results are again similar in both cases. The energies of the molecules are very small (<0.2 eV). Figure 9 shows the average energy of atomic deuterium and tritium incident on the outer wall and pumping duct.

The pressure at the end of the pumping duct is found from DEGAS to be 1.35×10^{-5} Pa. This does not com-

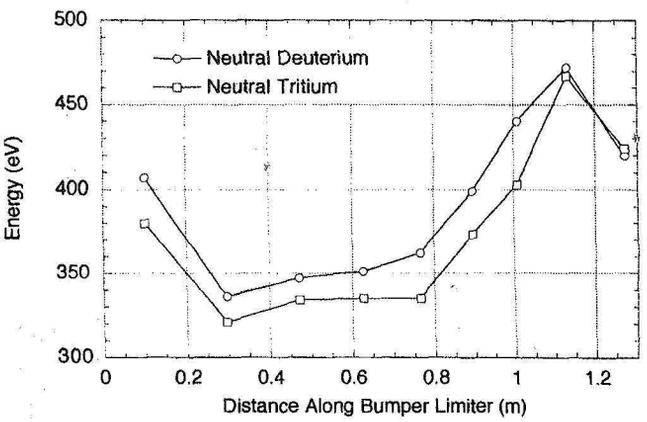

Fig. 8. Average energy of deuterium and tritium neutrals incident on the bumper limiter.

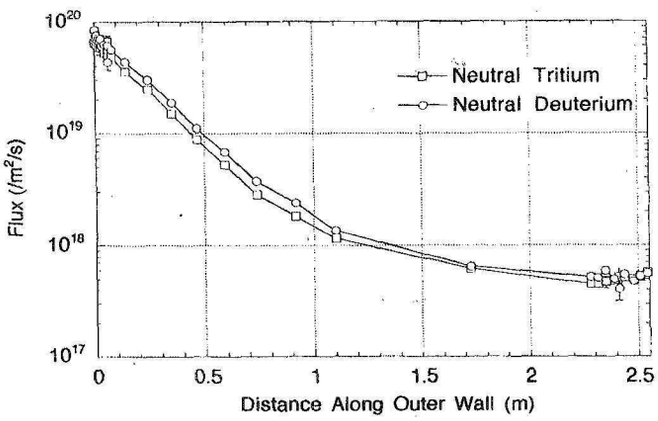

Fig. 6. Deuterium and tritium neutral fluxes to the outer wall and pumping duct.

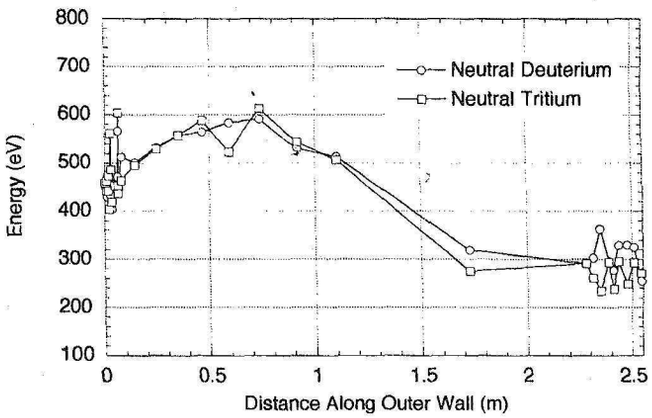

Fig. 9. Average energy of deuterium and tritium neutrals incident on the outer wall and pumping duct.

pare favorably with RGA data, which indicate a pressure of 1.2×10^{-3} Pa at this location. The main reason for this discrepancy is the fact that the DEGAS result is during the discharge, while the RGA data are only valid for after the discharge, when the pressure increases. Ion gauge pressure data during the discharge are around its noise level and are valid only as an upper limit, with a pressure somewhat below 1×10^{-4} Pa. The measured tritium pressure is three to ten times the gauge pressure, as ions not striking beam dump releases T_2 gas that flows out in to the torus.

The total energy distribution of particles reaching the bumper limiter has two peaks, one at 4 eV from molecular dissociation and the other on the order of 750 eV. Only the higher energy particles will implant into the walls to any significant degree. The reflection coefficient for either deuterium or tritium on carbon is ~0.09. (Whether one includes the effect of the lithium pellets and whether lithium is distributed on the bumper limiter is not important since the reflection coefficient is similar for a lithium or carbon target.) The deuterium current to the bumper limiter is $(1.38 \pm 0.02) \times 10^{22}$ s^{-1}, and the tritium current is $(1.27 \pm 0.02) \times 10^{22}$ s^{-1}. The implanted current is then found by taking the incident current times the percentage that does not reflect times the percentage of particles in the higher energy range. When this is done, the implanted currents are found to be $(6.03 \pm 0.08) \times 10^{21}$ s^{-1} and $(5.40 \pm 0.08) \times 10^{21}$ s^{-1} for deuterium and tritium, respectively. The deuterium current to the outer wall and pumping duct is $(1.95 \pm 0.029) \times 10^{21}$ s^{-1}, and the tritium current is $(1.96 \pm 0.038) \times 10^{21}$ s^{-1}. Similar calculations are performed for the iron outer wall, using a reflection coefficient of 0.54 (average energy of 405 eV) , and the corresponding results are $(9.97 \pm 0.01) \times 10^{20}$ s^{-1} and $(1.06 \pm 0.01) \times 10^{21}$ s^{-1} for deuterium and tritium, respectively.

For a calculation of in-vessel and duct inventory, the following loss mechanisms were considered. During the shot, particles can be implanted in the walls or escape (either out the duct or into the plasma or become ionized). After the shot they are pumped out.

Several materials properties were used. It is assumed that carbon is saturated at 0.4 D/C (Ref. 22). Thus, for every implanted particle one comes out. The stainless steel was assumed to be saturated at 0.01 D/Fe (Ref. 23). Also, the implantation range in carbon and iron were taken from TRIM but were multiplied by 1.8 to take into account saturation effects.[24] The bumper limiter area used is 23 m^2, and the outer wall and ducts are 110 m^2. Assuming a saturated wall and knowing the depth of implantation is sufficient information to calculate the retained tritium independent of the DEGAS simulation. However, since trapping in the codeposited layer is likely, the detailed knowledge of the fluxes and energies to the wall are useful quantities to know.

Putting all of the information together, it is estimated that the amount of tritium retained in the vacuum vessel from implantation after one hundred fifty 1-s discharges easily reaches saturation and is 0.5 ± 0.1 g, or 5 ± 1 kCi. The retention in the outer wall and duct is 0.042 ± 0.023 g, or 0.44 ± 0.19 kCi. These do not include deposition in a redeposited layer which could be removed by He/O discharge cleaning. It is seen that the total amount of implanted tritium is well below the total allowed limit of 5 g and below the ideal limit of 2 g of in-vessel inventory. Being well below the allowed level is important since the implanted tritium reaches fairly large depths and would be difficult to remove for recovery with mechanisms such as HeO glow discharge cleaning with a removal rate of only 0.01 nm/s.

V. SUMMARY

This paper shows experimental, analytical, and modeling results for the primary tritium pathway in TFTR—the neutral beams. Reasonable agreement was achieved between the measured inputs and the global modeling results. The model then shows the detailed behavior of the neutral gas in and around the beam box, pumping duct, torus edge, and bumper limiter. Finally the implanted inventory is estimated.

ACKNOWLEDGMENTS

We would like to thank D. Stotler at Princeton Plasma Physics Laboratory (PPPL) for help with DEGAS. This work is supported by the U.S. Department of Energy under contract S-03436, subcontracted through PPPL and by the Magnetic Fusion Energy Technology fellowship program.

REFERENCES

1. J. D. STRACHAN et al., *Phys. Rev. Lett.*, **72**, 3526 (1994).

2. K. M. McGUIRE et al., *Phys. Plasmas*, **2**, 2176 (1995).

3. C. H. SKINNER et al., *J. Nucl. Mater.* (to be published).

4. D. MUELLER et al., *J. Nucl. Mater.* (to be published).

5. L. C. PITTENGER, *Proc. 6th Symp. Engineering Problems of Fusion Research*, San Diego, California, 1975, p. 700, Institute of Electrical and Electronic Engineers, New York (1976).

6. L. C. PITTENGER, R. R. STONE, L. E. VALBY, and L. R. PEDROTTI, *Proc. 7th Symp. Engineering Problems of Fusion Research*, Knoxville, Tennessee, 1977, Vol. 1, p. 555, Institute of Electrical and Electronics Engineers, New York (1977).

7. M. C. VELLA, W. S. COOPER, P. A. PINCOSY, R. V. PYLE, P. D. WEBER, and R. P. WELLS, *Rev. Sci. Instrum.*, **59**, 2357 (1988).

8. S. K. ALLISON, *Rev. Mod. Phys.*, **30**, 1137 (1958).

9. J. KAMPERSCHROER, Unpublished internal Princeton Plasma Physics Laboratory memo.

10. J. H. KAMPERSCHROER et al., *Rev. Sci. Instrum.*, **66**, 632 (1995).

11. J. H. KAMPERSCHROER et al., *Rev. Sci. Instrum.*, **66**, 130 (1995).

12. D. HEIFETZ, D. POST, M. PETRAVIC, J. WEISHEIT, and G. BATEMAN, *J. Comput. Phys.*, **46**, 309 (1982).

13. D. HEIFETZ and D. POST, *Comp. Phys. Comrn.*, **29**, 287 (1983).

14. D. N. RUZIC and K. CHIU, *J. Nucl. Mater.*, **162–164**, 904 (1989).

15. D. N. RUZIC, *Nucl. Instrum. Methods*, **B47**, 118 (1990).

16. L. E. VALBY, *Proc. 7th Symp. Engineering Problems of Fusion Research*, Knoxville, Tennessee, 1977, Vol. 2, p. 1040, Institute of Electrical and Electronic Engineers, New York (1977).

17. J. A. SNIPES et al., *J. Nucl. Mater.*, **196/198**, 686 (1992).

18. R. V. BUDNY, D. COSTER, D. STOTLER, M. G. BELL, A. C. JANOS, and D. K. OWENS, *J. Nucl. Mater.*, **196/198**, 462 (1992).

19. M. C. ZARNSTORFF et al., *Phys. Fluids B*, **2**, 1852 (1990).

20. R. V. BUDNY et al., *Nucl. Fusion*, **32**, 429 (1992).

21. B. J. BRAAMS and C. E. SINGER, *Fusion Technol.*, **9**, 320 (1986).

22. K. L. WILSON, *J. Nucl. Mater.*, **145/147**, 121 (1987).

23. K. L. WILSON, *J. Nucl. Mater.*, **103/104**, 453 (1981).

24. S. K. ERENTS and E. S. HOSTON, *Nucl. Instrum. Methods*, **170**, 44 (1980).

Lisa A. Haynes (MS, nuclear engineering, University of Illinois, 1995) is a teaching assistant at the University of Illinois, Department of Nuclear Engineering. Her current research interests include transition flows in edge plasmas.

J. P. Kelly No biography was available at publication time.

David N. Ruzic (BS, physics, Purdue University, 1979; MA, 1981, and PhD, 1984, physics, Princeton University) is a professor in the Department of Nuclear Engineering and Physics, and Electrical and Computer Engineering at the University of Illinois at Urbana-Champaign. He works in both experimental and computational plasma material interactions for fusion and semiconductor processing applications.

Dennis Mueller (PhD, Michigan State University, 1976) is a principal research physicist at the Princeton University Plasma Physics Laboratory and is branch head for Physics Operations for the Tokamak Fusion Test Reactor (TFTR). His research interests include plasma control systems, plasma/wall interaction, and neutral beam heating of thermonuclear plasmas.

J. Kamperschroer No biography was available at publication time.